

Intrinsic anomalous spin Hall effect

Ping Li,^{1,2} Jing-Zhao Zhang,¹ Zhi-Xin Guo,^{1,2,*} Tai Min,¹ and X. R. Wang^{3,4,†}

¹State Key Laboratory for Mechanical Behavior of Materials,
Center for Spintronics and Quantum System, School of Materials Science and Engineering,
Xi'an Jiaotong University, Xi'an, Shaanxi, 710049, China

²Key Laboratory for Computational Physical Sciences (Ministry of Education), Fudan University, Shanghai, 200433, China

³Physics Department, The Hong Kong University of Science and Technology, Clear Water Bay, Kowloon, Hong Kong.

⁴HKUST Shenzhen Research Institute, Shenzhen 518057, China.

(Dated: August 11, 2022)

Charge-spin interconversion in magnetic materials is investigated by using first-principles calculations. In addition to the conventional spin Hall effect (SHE) that requires mutual orthogonality of the charge current, spin-flow direction, and spin polarization, the recently proposed anomalous SHE (ASHE) is confirmed in Mn₂Au and WTe₂. The interaction of the order parameter with conduction electrons leads to sizeable nonzero spin Berry curvatures that give rise to nonzero anomalous spin Hall conductivity (ASHC). Our calculations show that the ASHE is intrinsic and originates from the order-parameter-controlled spin-orbit interaction, which generates an extra anomalous effective field. A useful relationship among the order parameter, spin Berry curvature and ASHC is revealed. Our findings open a new avenue for arbitrary-type spin current generation and detection.

Keywords: anomalous spin Hall effect, spin Berry curvature, order parameter, spin-orbital coupling, spin-dependent electric field

PACS: 71.10.-d, 74.25.Ha, 75.30-m, 75.40.Cx

INTRODUCTION

The spin Hall effect (SHE) is related to spin current generation or spin accumulation from an electric current [1–4]. Different from an electric current, which is a flow of charges and a vector, a spin current, or an angular momentum flow, is a tensor of rank two with nine components in Cartesian coordinates. The SHE has attracted great attention and is widely used to generate a spin current, which is an indispensable component of spintronics [1–4]. The inverse SHE is a powerful method for detecting spin currents [5, 6].

In the SHE, a charge current along the $\hat{\beta}$ direction in a material with a strong spin-orbit interaction (SOI) can generate a spin current j_α^γ whose propagation and spin polarization are along the $\hat{\alpha}$ and $\hat{\gamma}$ directions, respectively. The conventional SHE requires $\hat{\alpha}$, $\hat{\beta}$, and $\hat{\gamma}$ to be mutually orthogonal to each other. Recently, Wang proposed that interactions of conduction electrons with order parameters, such as magnetization for ferromagnets and the Néel order for antiferromagnets, give rise to the anomalous SHE (ASHE) [7]. In linear response theory, spin current j_i^j due to charge current \mathbf{J} is given by

$$j_i^j = \frac{\hbar}{2e} \theta_{ijk}^{SH} J_k, \quad (1)$$

where θ_{ijk}^{SH} is the spin Hall angle tensor of rank 3. $i, j, k = 1, 2, 3$ denote the x, y, and z directions, and the Einstein summation notation is used. i, j , and k denote the spin current direction, spin polarization direction, and charge current direction. Based on the general tensor require-

ment of a physical quantity, one has [7]

$$\theta_{ijk}^{SH} = \theta_0 \epsilon_{ijk} + [(\theta_1 + \theta_2) \delta_{ij} \delta_{kl \neq i} + \theta_1 \delta_{ik} \delta_{jl \neq i} + \theta_2 \delta_{il} \delta_{jk \neq i}] M_l, \quad (2)$$

where M_l and ϵ_{ijk} are the l th component of \mathbf{M} and the Levi-Civita symbols, respectively. θ_0 is the usual spin Hall angle that does not depend on \mathbf{M} , while θ_1 and θ_2 are two ASHE coefficients. Thus, the conventional SHE is nonzero only when i, j , and k take different values. However, the terms involving M_l can be nonzero, which leads to nonzero ASHE spin currents, as indicated in Figs. 1f–1h. This newly proposed ASHE was not only directly verified by experiments of the anomalous spin torques generated in Mn₂Au [8] but also agreed with the details of the observed magnetization-dependent anomalous inverse SHE (AISHE) in a Pt/Co/Pt heterostructure [9], TbCo alloys [10], and Co/Pd multilayers [11]. The ASHE overcomes the limitation of the SHE, and the generated spin current can be controlled by order parameters. In particular, the ASHE allows the spin polarization and spin propagation directions to be collinear when the applied electric current is along the order parameter direction. Such a spin current can generate an out-of-plane anti-damping spin-orbit torque (SOT) that is crucial to realizing field-free switching of perpendicular magnetization in high-density SOT devices such as SOT-MRAM [12–17].

Although the ASHE concept has been widely recognized, its microscopic origin remains to be revealed. Recently, first-principles calculations [18, 19] were used to study the anomalous spin torques observed in experiments involving ferromagnets and antiferromagnets.

However, the discussions are limited to qualitative symmetry analysis [20], and the intrinsic mechanism of the ASHE is still elusive [21]. One cannot quantitatively compute the anomalous spin torques of specific materials without knowing the intrinsic mechanism. Such an investigation is particularly desirable in the field of high-performance SOT devices [14, 16, 21].

Using the local spin density approximation theory with the SOI, we investigate the intrinsic mechanism of the ASHE, with the following findings. 1) The ASHE originates from the order-parameter-induced extra spin-dependent electric field, which generates anomalous spin currents via the SOI. 2) The anomalous spin Hall conductivity (ASHC), which quantitatively represents the strength of the ASHE, can be well described by the spin Berry curvature. 3) There is an intrinsic connection among the order parameter, spin Berry curvature, and ASHC.

METHODS

Our spin-polarized density functional theory (DFT) calculations are performed using the Vienna *ab initio* Simulation Package (VASP) [22, 23] and QUANTUM ESPRESSO (QE) [24, 25], in which the projector augmented wave method and a plane-wave basis set are applied. We use the VASP for Mn_2Au and WTe_2 and QE for Fe. All calculations are performed using spin polarization within the framework of the local spin density approximation and generalized gradient approximation for the exchange-correlation energy. The electron exchange-correlation functional is described by the Perdew-Burke-Ernzerhof functional of the generalized gradient approximation [26]. The plane-wave cutoff energy is chosen to be 500 eV for Mn_2Au and WTe_2 and 120 Ry for Fe. Moreover, Γ -centered k meshes of $20 \times 20 \times 20$ (Pt), $16 \times 16 \times 16$ (Fe), $18 \times 9 \times 3$ (WTe_2), and $24 \times 24 \times 8$ (Mn_2Au) are adopted in the self-consistent calculations. To better describe the van der Waals (vdW) interaction, the optB86b-vdW functional is adopted for WTe_2 [27, 28]. Then, DFT wave functions are projected onto maximally localized Wannier functions using the WANNIER90 package [29], and the Kubo formula is applied to calculate the spin Hall conductivity (SHC) [30, 31]. Dense k -point meshes of $150 \times 150 \times 150$, $600 \times 600 \times 600$, $200 \times 200 \times 200$ and $150 \times 150 \times 150$ are employed for Pt, Fe, WTe_2 and Mn_2Au , respectively, to perform the Brillouin zone (BZ) integration for the SHC calculations with a careful convergence test.

RESULTS

According to local spin density approximation theory [32, 33], a position-dependent spin-dependent elec-

tric field $\vec{E}^p(\vec{r})$, which is proportional to the difference in the charge density gradients of spin-up and spin-down electrons, $[\nabla n^\uparrow(\vec{r})]$ and $[\nabla n^\downarrow(\vec{r})]$, can be induced by the magnetic order parameter \mathbf{M} (see Supporting Information). Note that the magnetization-induced spin-dependent electric field differs from the conventional electric field. The conventional electric field is defined as $\vec{E}(\vec{r}) = -[\nabla H^\uparrow(\vec{r}) + \nabla H^\downarrow(\vec{r})]$, while the spin-dependent electric field is defined as $\vec{E}^p(\vec{r}) = -[\nabla H^\uparrow(\vec{r}) - \nabla H^\downarrow(\vec{r})]$, where H^\uparrow and H^\downarrow are the Hamiltonians for spin-up and spin-down electrons, respectively. Hence, the spin-dependent electric field represents the difference in the electric fields between spin-up and spin-down electrons.

In a collinear magnetic structure with inversion symmetry, the effective spin-dependent electric field (averaged over the unit cell) defined as $\vec{E}_{eff}^p = \int \vec{E}^p(\vec{r}) d\vec{r} = 0$ is zero. However, \vec{E}_{eff}^p becomes nonzero if the inversion symmetry is broken. Such an \vec{E}_{eff}^p can induce an effective Hamiltonian H_{SOC}^{eff} via the SOI (see Supporting Information),

$$H_{SOC}^{eff} = \frac{\hbar e}{2mc^2} (\vec{\sigma} \times \vec{E}_{eff}^p) \cdot \vec{v}, \quad (3)$$

where $\vec{\sigma}$ and \vec{v} are the Pauli matrices and electron velocity, respectively. The nonzero H_{SOC}^{eff} means that the spin-up and spin-down electrons experience different forces and thus have different velocities. Hence, Eq. (3) leads directly to the ASHE as long as $\vec{\sigma}$ is perpendicular to \vec{E}_{eff}^p . For example, in a magnetic material without inversion symmetry in the \vec{z} direction, i.e., $E_{eff}^{pz} \neq 0$, one has nonzero $H_{SOC}^{eff} = \frac{\hbar e}{2mc^2} E_{eff}^{pz} (\sigma_y v_x - \sigma_x v_y)$. Thus, energy splitting between spin-up and spin-down electrons is generated by the SOI, leading to different velocities. As a result, anomalous spin currents with spin polarization perpendicular to \vec{z} , as predicted in Wang's theory [7], will be generated (see Supporting Information). Note that since the spin-dependent electric field directly correlates to the magnetic order parameter \mathbf{M} , nonzero E_{eff}^p is naturally expected in the direction of broken inversion symmetry induced by \mathbf{M} , rather than in the direction of the magnetic moment.

We find that the strength of the ASHE can be quantitatively described by the spin Berry curvature. According to the Kubo formula, the SHC $\sigma_{\alpha\beta}^\gamma$ of spin polarization direction $\hat{\gamma}$ and spin flow direction $\hat{\alpha}$ under an external electric field (charge current) along $\hat{\beta}$ can be expressed as [30, 31, 34, 35]

$$\sigma_{\alpha\beta}^\gamma = -\frac{e^2}{\hbar} \frac{1}{VN_k^3} \sum_k \sum_n f_{nk} \Omega_{n,\alpha\beta}^\gamma(\mathbf{k}), \quad (4)$$

where V is the cell volume and N_k^3 is the number of k points in the BZ. f_{nk} represents the Fermi-Dirac distribution function, and $\Omega_{n,\alpha\beta}^\gamma(\mathbf{k})$ is the band-projected spin Berry curvature, defined as

$$\Omega_{n,\alpha\beta}^\gamma(\mathbf{k}) = \hbar^2 \sum_{m \neq n} \frac{-2\text{Im}[\langle n\mathbf{k} | \frac{1}{2}\{\hat{\sigma}_\gamma, \hat{v}_\alpha\} | m\mathbf{k}\rangle \langle m\mathbf{k} | \hat{v}_\beta | n\mathbf{k}\rangle]}{(\epsilon_{n\mathbf{k}} - \epsilon_{m\mathbf{k}})^2}. \quad (5)$$

From Eqs. (4) and (5), one can see that the Hall conductivity $\sigma_{\alpha\beta}^\gamma$ is intrinsically determined by the band structure through the spin Berry curvature $\Omega_{n,\alpha\beta}^\gamma(\mathbf{k})$ and density of states. In the conventional SHE, nonzero $\Omega_{n,\alpha\beta}^\gamma(\mathbf{k})$ is expected only when α , β and γ are mutually orthogonal to each other. However, as discussed below for the case involving the order parameter, nonzero $\Omega_{n,\alpha\beta}^\gamma(\mathbf{k})$ and thus a sizeable ASHE can also be obtained when only two of them are mutually perpendicular. In addition, the general Berry curvature formula, which requires $\alpha \neq \beta$, was derived by simply considering the spin direction perpendicular to the velocities of the spin current and charge current ($\alpha \neq \beta \neq \gamma$) [36]. In this case, the spin degree of freedom is not effectively considered, and the Berry curvature is in fact a tensor of rank 2. However, in the definition of spin Berry curvature shown in Eq. (5), the interaction between the spin degree of freedom and spin current is effectively considered via the anticommutator operator. As a result, the spin Berry curvature becomes a tensor of rank 3, which is nonzero even for $\alpha = \beta$.

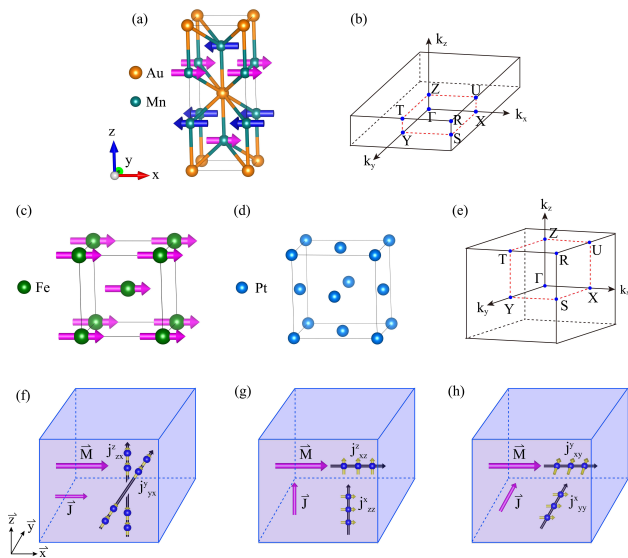


FIG. 1. **Atomic structures, schematic diagrams of the BZs, and schematic diagrams of the ASHE.** (a), (c) and (d) show the atomic structures of TET Mn_2Au , BCC Fe and FCC Pt, respectively. (b) and (e) show the corresponding BZs. Note that BCC Fe and FCC Pt have the same BZ structure, shown in (e). (f) illustrates the ASHE with charge current \vec{J} parallel to order parameter \vec{M} , and (g, h) present the ASHE with charge current \vec{J} perpendicular to \vec{M} .

We first consider tetragonal (TET) Mn_2Au as an illustration, whose nonzero ASHE has been experimentally

observed [8]. We systematically show below an intrinsic connection among the order parameter, spin Berry curvature and ASHE. DFT calculations were performed to obtain the spin Berry curvature and SHC (see Supporting Information). The crystal structure and schematic BZ diagram of Mn_2Au are illustrated in Figs. 1a and 1b, which verify that Mn_2Au is an antiferromagnetic material with a Néel order parameter \vec{M} . In this study, \vec{M} is fixed in the \vec{x} direction. Hence, as indicated in Figs. 1e-1g, six nonzero ASHCs are expected, that is, σ_{yx}^y and σ_{zx}^z for charge current \vec{J} parallel to \vec{M} and σ_{zx}^x , σ_{xz}^z , σ_{yy}^x , and σ_{xy}^y for \vec{J} perpendicular to \vec{M} [7].

The calculated components of both the conventional SHC (CSHC) and ASHC are shown in Table I. In addition to the large CSHCs, there are also sizeable ASHCs in Mn_2Au . Moreover, both CSHCs and ASHCs exhibit significant anisotropy, depending on the combination of the spin current, spin polarization, and charge current directions. This characteristic is quite different from that of the conventional SHE, whose anisotropy arises solely from the crystalline structure [20]. For instance, the symmetry of Mn_2Au is expected to give rise to the same CSHCs for σ_{xy}^z and σ_{yx}^z . However, the former [270.58 (\hbar/e) S/cm] is more than 3 times larger than the latter [-81.11 (\hbar/e) S/cm] because of the broken fourfold rotational symmetry due to \vec{M} along the \vec{x} direction.

Moreover, \vec{M} along the \vec{x} direction in Mn_2Au can lead to an additional nonzero spin-dependent electric field in the \vec{z} direction (E_z^p) due to its broken inversion symmetry. According to Eq. (3), the nonzero E_z^p would induce a spin current with spin polarization in both the \vec{x} and \vec{y} directions via the SOI and thus leads to sizeable ASHCs. The details are given in the Supporting Information. Our DFT calculations indeed show that the absolute values of ASHCs with spin polarization in the \vec{x} direction (σ_{zx}^x , σ_{yy}^x) and \vec{y} direction (σ_{yx}^y , σ_{xy}^y) are significantly larger than those with spin polarization in the \vec{z} direction (σ_{zx}^z , σ_{xz}^z) (Table I). The nonzero values of σ_{zx}^z and σ_{xz}^z may be from other ASHE mechanisms that are beyond the scope of effective field theory discussed above. Among the six ASHC components, the largest component is σ_{yx}^y [15.57 (\hbar/e) S/cm], the magnitude of which reaches 19% of that of its conventional counterpart σ_{yx}^z [-81.11 (\hbar/e) S/cm]. Thus, a sizeable spin current, whose propagation direction is collinear to the spin polarization direction, can be effectively generated in Mn_2Au . This result is consistent with the experiments [8]. The good agreement between our theoretical derivations and DFT calculations verifies the intrinsic connection among the order parameter, spin Berry curvature and ASHE.

As a comparison, we also calculated the SHCs of bulk

TABLE I. **Spin Hall Conductivity.** Calculated CSHCs and ASHCs for Fe, Mn₂Au and Pt. Each SHC is denoted as $\sigma_{\alpha\beta}^{\gamma}$, where α is the direction of the spin current, β is that of the applied electrical field and γ is that of the spin polarization of the spin current (unit: $(\hbar/e)S/cm$). The magnetic order parameter \mathbf{M} is fixed to be along the \vec{x} direction for Fe and Mn₂Au.

	SHC	Mn ₂ Au	Fe	Pt
CSHC	σ_{xy}^z	270.58	120.76	2239.42
	σ_{yx}^z	-81.11	-683.71	-2239.58
	σ_{yx}^y	15.57	2.87	0.00
	σ_{zx}^z	0.02	-2.89	0.00
ASHC	σ_{zz}^x	-10.46	-0.66	0.00
	σ_{xz}^z	-2.95	-3.14	0.00
	σ_{yy}^y	-6.72	0.49	0.00
	σ_{xy}^y	-9.09	1.37	0.00

Fe in the body-centered cubic (BCC) structure. As shown in Fig. 1(c), although a large \mathbf{M} exists along the \vec{x} direction, \vec{E}^p in this system is zero due to the inversion symmetry (see Supporting Information). This means that the order parameter does not directly induce the ASHE in BCC Fe. Our DFT calculations show that despite its considerably large CSHCs, all the ASHCs in Fe are very small, with an ASHC/CSHC ratio of less than 0.5% (Table I). We also explored the SHCs of nonmagnetic Pt in the face-centered cubic (FCC) structure. As shown in Table I, although the CSHCs of Pt are larger than those of Mn₂Au by an order of magnitude, all its ASHCs are negligible [$<10^{-3}$ $(\hbar/e)S/cm$]. This result confirms the intrinsic connection between the order parameter and ASHE.

As discussed in the Supporting Information, the exchange-correlation potential between spin-up and spin-down electrons in the Kohn-Sham equations depends on the magnetic order parameter (see Supporting Information). Thus, the spin-polarized DFT calculations under the local spin density approximation can be used to study order parameter effects on exchange interactions and SOIs [32, 33]. Hence, the calculated electronic structures, such as band structures and wave functions, contain the effects of the order parameter. Since the spin Berry curvature is directly calculated on the basis of electronic structures [Eq. (5)], this shows an intrinsic connection of the ASHE to the spin Berry curvature. In fact, the intrinsic connection between the spin Berry curvature and conventional SHE was also well justified in previous studies [36–38].

We further computed the k -resolved spin Berry curvatures for both CSHCs (a, c, e in Fig. 2) and ASHCs (b, d, f in Fig. 2) of bulk Mn₂Au, Fe, and Pt. A common feature is that the spin Berry curvatures for ASHCs are much smaller than those for CSHCs, which agrees with the experimental fact that the ASHCs in these materials are smaller than the CSHCs. In addition, positive and negative spin Berry curvatures coexist in the BZ, and

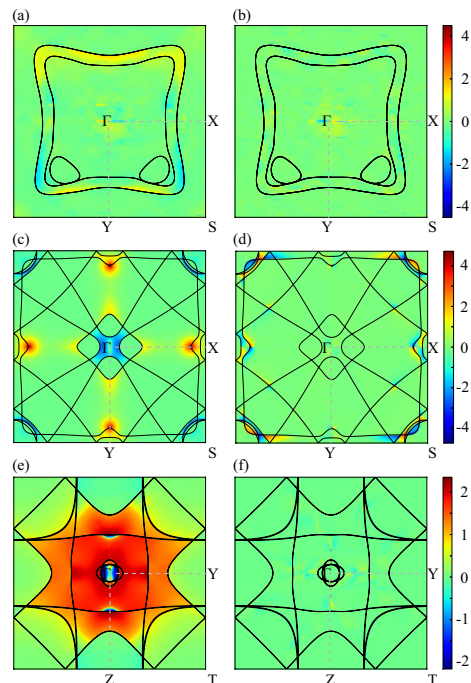


FIG. 2. **Spin Berry curvature in BZ slices.** Density plots of the spin Berry curvature in the BZ slice of $k_z = 0$ for bulk Mn₂Au (a, b) and Fe (c, d) and the 2D BZ of $k_x = 0$ for Pt (e, f). (a), (c), and (e) are the spin Berry curvature for CSHCs: σ_{yx}^z of Mn₂Au, σ_{xy}^z of Fe, and σ_{xy}^z of Pt, respectively. (b), (d), and (f) are the spin Berry curvature for ASHCs: σ_{yx}^y of Mn₂Au (b), σ_{yx}^y of Fe (d), and σ_{yx}^y of Pt (f). The black lines denote the intersections of the Fermi surface with the slices. The color code is on the log scale.

both CSHC and ASHC values are determined by the sum of all k points. Thus, although the spin Berry curvature value of Fe is larger than that of Mn₂Au throughout the BZ, its ASHC is much smaller than that of Mn₂Au due to the cancellation of positive and negative spin Berry curvatures. This result also agrees well with the symmetry analysis above. For Pt, the spin Berry curvatures for the CSHC are dominated by regions with large positive values, while those for ASHC are tiny with equal weights on the positive and negative values, leading to the largest CSHC and a negligible ASHC in comparison with those of Mn₂Au and Fe. The calculated Hall conductivities shown in Table I are in good agreement with these spin Berry curvatures profiles. The above results clearly show that the spin Berry curvature is intrinsically connected not only to the conventional SHE but also to the ASHE.

DISCUSSION AND CONCLUSION

The ASHE is not limited to the magnetic order parameter; any order parameter breaking the inversion symmetry can lead to nonzero ASHC via the SOI (such effect in

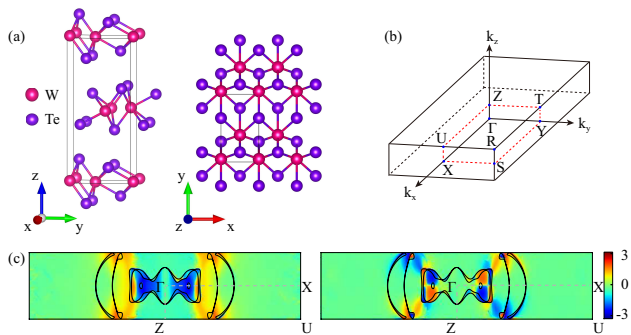


FIG. 3. **Atomic structure, BZ, and spin Berry curvature of WTe₂.** Atomic structure (a), schematic diagram of the BZ (b), and k -resolved spin Berry curvature on a log scale in a slice of the 2D BZ at $k_y = 0$ (c) for bulk WTe₂. The left and right panels in (c) show the spin Berry curvature for σ_{zx}^z and σ_{zy}^z , respectively. The black lines show the intersections of the Fermi surface with a slice of the BZ.

nonmagnetic materials is denoted as the unconventional SHE). For example, the crystal structure of nonmagnetic material T_d-WTe₂ [Fig. 3(a)] breaks the mirror symmetry with respect to the xz plane and thus leads to broken inversion symmetry. The broken symmetry in this case induces a nonzero conventional electric field in the \vec{y} direction (E_{eff}^y). According to the SOI Hamiltonian presented in Eq. (3), a sizable unconventional SHE spin current can still be generated when the spin polarization direction is perpendicular to \vec{y} (see Supporting Information). To verify this, we performed DFT calculations on the spin Berry curvature and ASHC of WTe₂ and found $\sigma_{zx}^z = 18.99$ (\hbar/e) S/cm , reaching 18% of its conventional SHC counterpart σ_{zx}^y [103 (\hbar/e) S/cm] [39]. However, we found that σ_{zy}^z has a much smaller value [2.08 (\hbar/e) S/cm], which may be attributed to the indirect interaction between E_{eff}^y and v_y . This result is consistent with experimental observations, where field-free switching of perpendicular magnetization was observed only with charge current in the \vec{x} direction and not in the \vec{y} direction [14, 40, 41]. In addition, as shown in Fig. 3, the positive spin Berry curvature for σ_{zx}^z is much larger than that for σ_{zy}^z . This result confirms the intrinsic connection between the spin Berry curvature and unconventional SHE in nonmagnetic materials.

In addition, we would like to discuss the novelty of this work in comparison with previous studies [19, 20, 42–44]. The notion of the ASHE was first proposed for spin current generation in a ferromagnet from an AHE-induced charge current through the conventional SHE (a phenomenon of SHE+AHE) [19, 42, 43]. However, the ASHE in our study resulted from the combined effect of the order parameter and SOI. The physical origins of the two theories are fundamentally different. Moreover, the two theories make distinct predictions: The ASHE in Refs. 19, 42, and 43 predicts a nonzero spin current

only for the noncollinear magnetic order parameter and external electric field. In contrast, the ASHE in this work additionally predicts that the collinear order parameter and charge current generate a spin current with collinear propagation direction and polarization. Unconventional components of the SHC tensor were also discussed in Ref. 20 from the symmetry restriction point of view. Their analysis is valid only when the order parameter is not involved in spin-charge conversion, in contradiction to the ASHE in this work. In fact, the analysis of Ref. 20 fails to give rise to the ASHC component in Mn₂Au observed in experiments [8]. Note also that order parameter dependence of the conventional SHE and AHE in ferromagnets was recently observed in ferromagnets [44].

Before closing, we would like to emphasize that a dense k -point mesh setting is necessary to guarantee the reliability of the SHC and ASHC calculations. For example, in Fig. S1 of the Supporting Information, we show the ASHC σ_{xy}^y of Fe calculated with various k -point mesh settings. Clearly, σ_{xy}^y is as large as 183.48 (\hbar/e) S/cm for a small k -point mesh of $50 \times 50 \times 50$ while its converged value is approximately 1.0 (\hbar/e) S/cm , which can be obtained when the k -point mesh is larger than $400 \times 400 \times 400$. Therefore, the k -point mesh convergence test is crucial to the Hall conductivity calculations.

In summary, we have revealed the nature of the intrinsic ASHE: The ASHE originates from the order-parameter-induced spin-dependent electric field, which generates a spin current via the SOI. The intrinsic relationship among the order parameter, spin Berry curvature and ASHE is also revealed. The effects of the order parameter on the electronic structure lead to a nonzero spin Berry curvature and thus a sizeable ASHE. The order parameter that gives rise to the ASHE is not limited to the magnetic order parameter. Any order parameter that can lead to broken inversion symmetry should contribute to the ASHE. This study is expected to provide an efficient way to search for and optimize materials with large ASHE, which is particularly important in the design of high-performance SOT spintronic devices.

We thank Prof. Jian Zhou and Dr. Yongliang Shi for valuable discussions. This work is supported by the National Natural Science Foundation of China (No. 12074301, 12004295, and 11974296) and Hong Kong RGC Grants (No. 16300522, 16301619, and 16302321). P. Li thanks China's Postdoctoral Science Foundation funded project (No. 2020M673364) and the Open Project of the Key Laboratory of Computational Physical Sciences (Ministry of Education). This research used the resources of the HPCC platform in Xi'an Jiaotong University.

SUPPORTING INFORMATION

The supporting information is available online. The supporting materials are published as submitted, without typesetting or editing. The responsibility for scientific accuracy and content remains entirely with the authors.

* zxguo08@xjtu.edu.cn

† phxwan@ust.hk

- [1] S. Murakami, N. Nagaosa, and S. C. Zhang, *Science* **301**, 1348 (2003).
- [2] J. Sinova, D. Culcer, Q. Niu, N. A. Sinitsyn, T. Jungwirth, and A. H. MacDonald, *Phys. Rev. Lett.* **92**, 126603 (2004).
- [3] J. Sinova, S. O. Valenzuela, J. Wunderlich, C. H. Back, and T. Jungwirth, *Rev. Mod. Phys.* **87**, 1213 (2015).
- [4] J. E. Hirsch, *Phys. Rev. Lett.* **83**, 1834 (1999).
- [5] B. F. Miao, S. Y. Huang, D. Qu, and C. L. Chien, *Phys. Rev. Lett.* **111**, 066602 (2013).
- [6] J. C. Rojas-Sanchez, N. Reyren, P. Laczkowski, W. Savero, J. P. Attane, C. Deranlot, M. Jamet, J. M. George, L. Vila, and H. Jaffres, *Phys. Rev. Lett.* **112**, 106602 (2014).
- [7] X. R. Wang, *Commun. Phys.* **4**, 55 (2021).
- [8] X. Chen, S. Shi, G. Shi, X. Fan, C. Song, X. Zhou, H. Bai, L. Liao, Y. Zhou, H. Zhang, A. Li, Y. Chen, X. Han, S. Jiang, Z. Zhu, H. Wu, X. Wang, D. Xue, H. Yang, and F. Pan, *Nat. Mater.* **20**, 800 (2021).
- [9] T. C. Chuang, D. Qu, S. Y. Huang, and S. F. Lee, *Phys. Rev. Research* **2**, 032053(R) (2020).
- [10] A. Yagmur, S. Sumi, H. Awano, and K. Tanabe, *Phys. Rev. B* **103**, 214408 (2021).
- [11] M. Yang, B. Miao, J. Cheng, K. He, X. Yang, Y. Zeng, Z. Wang, L. Sun, X. Wang, A. Azevedo, S. Bedanta, and H. Ding, *Phys. Rev. B* **105**, 224426 (2022).
- [12] M. Cubukcu, O. Boule, M. Drouard, K. Garello, C. A. Onur, I. M. Miron, J. Langer, B. Ocker, P. Gambardella, and G. Gaudin, *Appl. Phys. Lett.* **104**, 042406 (2014).
- [13] L. Liu, C. F. Pai, Y. Li, H. W. Tseng, D. C. Ralph, and R. A. Buhrman, *Science* **336**, 555 (2016).
- [14] D. MacNeill, G. M. Stiehl, M. H. D. Guimaraes, R. A. Buhrman, J. Park, and D. C. Ralph, *Nat. Phys.* **13**, 330 (2017).
- [15] R. Ramaswamy, J. M. Lee, K. Cai, and H. Yang, *Appl. Phys. Rev.* **5**, 031107 (2018).
- [16] L. Liu, C. Zhou, X. Shu, C. Li, T. Zhao, W. Lin, J. Deng, Q. Xie, S. Chen, J. Zhou, R. Guo, H. Wang, J. Yu, S. Shi, P. Yang, S. Pennycook, A. Manchon, and J. Chen, *Nat. Nanotechnol.* **16**, 277 (2021).
- [17] Y. Zhang, H. Y. Yuan, X. S. Wang, and X. R. Wang, *Phys. Rev. B* **97**, 144416 (2018).
- [18] Y. Zhang, Y. Sun, H. Yang, J. Železný, S. P. P. Parkin, C. Felser, and B. Yan, *Phys. Rev. B* **95**, 075128 (2017).
- [19] V. P. Amin, J. Li, M. Stiles, and P. Haney, *Phys. Rev. B* **99**, 220405(R) (2019).
- [20] M. Seemann, D. Ködderitzsch, S. Wimmer, and H. Ebert, *Phys. Rev. B* **92**, 155138 (2015).
- [21] S. Lee, J. Ryu, and B.-G. Park, *Nat. Nanotechnol.* **16**, 226 (2021).
- [22] G. Kresse, and J. Hafner, *Phys. Rev. B* **47**, 558 (1993).
- [23] G. Kresse, and D. Joubert, *Phys. Rev. B* **59**, 1758 (1999).
- [24] P. Giannozzi, S. Baroni, N. Bonini, M. Calandra, R. Car, C. Cavazzoni, D. Ceresoli, G. L. Chiarotti, M. Cococcioni, I. Dabo, A. D. Corso, S. Gironcoli, S. Fabris, G. Fratesi, R. Gebauer, U. Gerstmann, C. Gougousis, A. Koalj, M. Lazzeri, L. Martin-Samos, N. Marzari, F. Mauri, R. Mazzarello, S. Paolini, A. Pasquarello, L. Paulatto, C. Sbraccia, S. Scandolo, G. Sclauzero, A. Seitsonen, A. Smogunov, P. Umari, and R. Wentzcovitch, *J. Phys.: Condens. Matter* **21**, 395502 (2009).
- [25] P. Giannozzi, O. Andreussi, T. Brumme, O. Bunau, M. B. Nardelli, M. Calandra, R. Car, C. Cavazzoni, D. Ceresoli, M. Cococcioni, N. Cococcioni, N. Colonna, I. Carnimeo, A. Corso, S. Gironcoli, P. Delugas, R. DiStasio Jr, A. Ferretti, A. Floris, G. Fratesi, G. Fugallo, R. Gebauer, U. Gerstmann, F. Giustino, T. Gorni, J. Jia, M. Kawamura, H-Y Ko, A. Kokalj, E. Kucukbenli, M. Lazzeri, M. Marsili, N. Marzari, F. Mauri, N. Nguyen, H-V Nguyen, A. Otero-de-la-Roza, L. Paulatto, S. Ponce, D. Rocca, R. Sabatini, B. Santra, M. Schlipf, A. Seitsonen, A. Smogunov, I. Timrov, T. Thonhauser, P. Umari, N. Vast, X. Wu, and S. Baroni, *J. Phys.: Condens. Matter* **29**, 465901 (2017).
- [26] J. P. Perdew, K. Burke, and M. Ernzerhof, *Phys. Rev. Lett.* **77**, 3865 (1996).
- [27] M. Dion, H. Rydberg, E. Schroder, D. C. Langreth, and B. I. Lundqvist, *Phys. Rev. Lett.* **92**, 246401 (2014).
- [28] J. Klimes, D. R. Bowler, and A. Michaelides, *Phys. Rev. B* **83**, 195131 (2011).
- [29] G. Pizzi, V. Vitale, R. Arita, S. Blugel, F. Freimuth, G. Geranton, M. Gibertini, D. Gresch, C. Jognson, T. Koretsune, J. I. Azpiroz, H. Lee, J. M. Lihm, D. Marchand, A. Marrazzo, Y. Mokrousov, J. I. Mustafa, Y. Nohara, Y. Nomura, L. Paulatto, S. Ponce, T. Ponweiser, J. Qiao, F. Thole, S. S. Tsirkin, M. Wierzbowska, N. Marzari, D. Vanderbilt, I. Souza, A. A. Mostofi, and J. R. Yates, *J. Phys.: Condens. Matter* **32**, 165902 (2020).
- [30] G. Y. Guo, Y. Yao, and Q. Niu, *Phys. Rev. Lett.* **94**, 226601 (2005).
- [31] J. Qiao, J. Zhou, Z. Yuan, and W. Zhao, *Phys. Rev. B* **98**, 214402 (2018).
- [32] R. Zeller, *Comput. Nanosci.* **31**, 419 (2006).
- [33] H.-A. Engle, E. I. Rashba, B. I. Halperin, in *Handbook of Magnetism and Advanced Magnetic Materials* edited by H. Kronmüller and S. Parkin (Wiley, Chichester, UK, 2007), Vol. V, pp. 3-4.
- [34] Q. Lu, P. Li, Z. Guo, G. Dong, B. Peng, X. Zha, T. Min, Z. Zhou, and M. Liu, *Nat. Commun.* **13**, 1650 (2022).
- [35] L. Salemi, and P. M. Oppeneer, *Phys. Rev. B* **106**, 024410 (2022).
- [36] D. Xiao, M. C. Chang, and Q. Niu, *Rev. Mod. Phys.* **82**, 1959 (2010).
- [37] Y. Yao, L. Kleinman, A. H. MacDonald, J. Sinova, T. Jungwirth, D. S. Wang, E. Wang, and Q. Niu, *Phys. Rev. Lett.* **92**, 037204 (2004).
- [38] N. Nagaosa, J. Sinova, S. Onoda, A. H. MacDonald, and N. P. Ong, *Rev. Mod. Phys.* **82**, 1539 (2010).
- [39] J. Zhou, J. Qiao, A. Bournel, and W. Zhao, *Phys. Rev. B* **99**, 060408(R) (2019).
- [40] B. Zhao, B. Karpiak, D. Khokhriakov, A. Johansson, A. M. Hoque, X. Xu, Y. Jiang, I. Mertig, and S. P. Dash, *Adv. Mater.* **32**, 2000818 (2020).

- [41] I. Kao, R. Muzzio, H. Zhang, M. Zhu, J. Gobbo, D. Weber, R. Rao, J. Li, J. H. Edgar, J. E. Goldberger, J. Yan, D. G. Mandrus, J. Hwang, R. Cheng, J. Katoch, and S. Singh, *arXiv: 2021.12388* (2021).
- [42] T. Taniguchi, J. Grollier, and M. D. Stiles, *Phys. Rev. Appl.* **3**, 044001 (2015).
- [43] K. S. Das, W. Y. Schoemaker, B. J. van Wees, and I. J. Vera-Marun, *Phys. Rev. B* **96**, 220408(R) (2017).
- [44] G. Qu, K. Nakamura, and M. Hayashi, *Phys. Rev. B* **102**, 144440 (2020).